JOURNAL OF AIRCRAFT
Vol. 35, No. 3, May–June 1998

Coupled Navier–Stokes and Optimizer Analysis of a Transonic Wing

Roxana M. Greenman*
NASA Ames Research Center, Moffett Field, California 94035
Samson Cheung†
MCAT, Inc., Moffett Field, California 94035
and
Eugene L. Tu‡
NASA Ames Research Center, Moffett Field, California 94035

One of the challenges of wing design is knowing how the geometric parameters affect the aerodynamics in a given flight regime. This study demonstrates the use of a numerical optimization routine to understand the significance of changing different geometric parameters, e.g., wing planform, on the aerodynamic characteristics, such as the lift-to-drag ratio (*L*/*D*). A numerical optimization routine is integrated with a grid generator and a computational fluid dynamics Navier–Stokes flow solver. The geometric parameters studied are wing sweep, twist angle at the root, and twist angle at the tip. These geometric parameters are then analyzed to show how each one contributes to the *L*/*D* performance of a wing. By using the developed tool to examine the characteristics of a transonic wing, the engineer can develop a better understanding of the related flow physics and design a better performing wing. The results of this paper show that proper optimization may require a series of local optimization and angle-of-attack adjustments. Furthermore, it was found that multiple-design variable optimization yielded improved results over a single dominant design variable.

Nomenclature

AR = aspect ratio, b^2/S
b = wingspan
C_D = drag coefficient, $D/q_\infty S$
C_L = lift coefficient, $L/q_\infty S$
C_p = pressure coefficient, $(p - p_\infty)/q_\infty$
c = streamwise local chord of wing
D = drag force
D/L = drag-to-lift-ratio
L = lift force
L/D = lift-to-drag ratio
M = Mach number
mac = mean aerodynamic chord of wing
p = pressure
q_∞ = freestream dynamic pressure, $\frac{1}{2}\rho_\infty V_\infty^2$
Re_{mac} = Reynolds number based on freestream conditions, $\rho_\infty V_\infty \text{mac}/\mu_\infty$
S = wing planform area
t = thickness
V = velocity
x, y, z = Cartesian physical space coordinates
α = angle of attack
η = percent span station, $y/(b/2) \times 100$
θ = wing section local incidence angle
Λ = wing sweep angle
λ = wing taper ratio, c_t/c_r
μ = coefficient of viscosity
ρ = density

Subscripts
r = wing root
t = wing tip
∞ = freestream conditions

Presented as Paper 96-2486 at the AIAA 14th Applied Aerodynamics Conference, New Orleans, LA, June 17–20, 1996; received Oct. 2, 1996; revision received Dec. 20, 1997; accepted for publication Dec. 31, 1997.

*Aerospace Engineer, Applied Computational Aerodynamics Branch. Member AIAA.
†Senior Research Scientist; currently at MRJ Technology Solutions Inc., Moffett Field, CA 94035. Member AIAA.
‡Deputy Program Manager, Information Technology. Senior Member AIAA.

Introduction

COMPUTATIONAL techniques for aerodynamic design have improved considerably in recent years. Optimization methods have been developed that provide efficient means for improving the design process. Not only can optimization improve performance but it can also help in the understanding of the flow physics about a configuration. Optimization can be used as a tool to understand how the geometric parameters affect the aerodynamics.

In the past, there have been many approaches in developing aerodynamic numerical optimization to improve aircraft performance.[1] Most of these approaches can be categorized into two types: 1) indirect and 2) direct numerical optimization methods.[2] The indirect or inverse design method calculates the geometry from the prescribed aerodynamic distribution, usually the pressure distribution. The quality of the optimized shape depends on how well the distribution is defined. This can lead to problems in translating the design goals into properly defined distributions[3] containing the required aerodynamic characteristics. In addition, the inverse design method does not easily handle geometric constraints.

The second class of the optimization method is the direct aproach. In this approach an aerodynamic analysis code is coupled with a numerical optimizer to minimize a given aerodynamic objective function. Often this is accomplished by means of gradient evaluations.[4,5] The geometry of the body that is

being optimized can be represented by a general function or by parameters that define the body. The desired shape of the body is found by iterating directly on the geometry until a local minimum in the objective function is reached. Two fast methods for performing the gradient evaluations are finite differencing and analytical sensitivity methods. Examples of the analytical methods include the one-shot method[6] and the adjoint method (also called the control-theory method).[7,8] The one-shot method uses a multigrid technique to solve for the unknowns simultaneously, while restricting optimization on a design variable to grids that only produce nonsmooth perturbations. On the other hand, the adjoint method solves the adjoint equation of the Navier–Stokes equations to obtain the sensitivity direction. Because the analytic methods typically employ modifications to the governing equations in the computational fluid dynamics (CFD) code, they require recoding of the flow solvers, objective functions, and boundary conditions. Unfortunately, these methods cannot take advantage of existing validated analysis codes. In this paper, the finite difference method is used for the gradient evaluation.

The purpose of this present study is to investigate transonic wing design by using numerical optimization as a tool to examine the geometric effects on wing performance. This is accomplished by integrating a grid generator, an existing CFD analysis code that solves the three-dimensional Navier–Stokes equations, and a quasi-Newton numerical optimization code. The resulting code complex streamlines the optimization procedure. For each optimization iteration the code automatically modifies the geometry, regenerates the surface and volume grids, and executes the flow solver.

The geometry that is chosen for this study is the Lockheed wing A,[9] which is representative of an advanced transport aircraft concept. There has been extensive wind-tunnel tests and numerical research conducted on this wing in the past.[5,9] The current flow solver is validated by comparing the numerical results with the experimental data obtained in the Lockheed Compressible Wind Tunnel Experiment.[9] In this study the optimizer is used as a tool to understand the flow physics about this wing with the goal of maximizing the L/D.

A brief discussion of the numerical approach is presented in the next section, including grid generation, the governing equations, and the flow solver. Next, the optimization procedure is discussed, including the numerical optimizer, design variables, nonlinear constraint, and objective function. The results are then presented, from which the effectiveness of the optimizer as a tool in aerodynamic design is discussed.

Numerical Approach

Geometry Definition

Extensive wind-tunnel investigations have been carried out by Hinson and Burdges[9] for the transonic wing shown in Fig. 1. This wing, referred to as wing A, has a planform that is representative of an advanced transport aircraft concept. Two control stations at the root and tip are used to define wing A. Geometrical specifications of this wing include a semispan of $b/2$ = 18 in., half-wing planform area of $S/2$ = 81.8 in.^{2}, an aspect ratio of AR = 8.0, and a leading-edge sweep of Λ = 27.0 deg. The mean aerodynamic chord is mac = 4.825 in. The wing contains a linear twist distribution where the twist angles

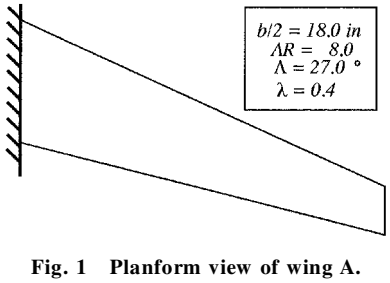

Fig. 1 Planform view of wing A.

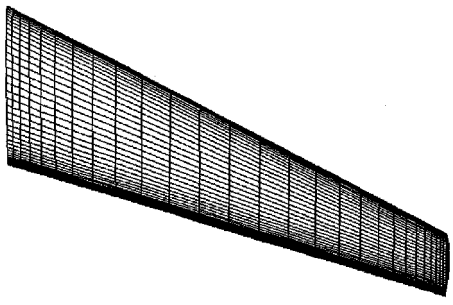

Fig. 2 Surface grid, 201 × 63 × 63 points (every other point shown for clarity).

at the root and tip are θ_r = 2.76 deg and θ_t = −2.04 deg, respectively. The thickness at both the root and tip are t/c = 12%.

Grid Generation

A surface grid is generated by using the root and tip airfoils as control stations and the wing planform parameters as variables. During the optimization procedure these planform variables can be directly specified by the optimizer for regridding of the geometry. Linear interpolation and hyperbolic tangent stretching are used to create the surface points in the streamwise and spanwise direction. A wing tip is added by adding a small cap that follows the curvature of the wing. The span of the wing-tip cap is b_t = 0.01 in., which is very small in comparison to the span of the wing. Having the surface grid defined, a three-dimensional hyperbolic grid generator[10] is used to generate the volume grid for the wing geometry. In this study, two different grid systems are used, a coarse grid and a refined grid. The coarse grid consists of 121 points in the streamwise direction, 39 points in the spanwise direction, and 43 points in the body-normal direction; whereas the refined grid, shown in Fig. 2, consists of 210 × 63 × 63 points, respectively. The initial normal direction spacing is 1.0×10^{-5} in. and the grid extends out in the normal direction nine mean aerodynamic chord lengths. The surface grid is clustered, as illustrated in Fig. 2, in regions where the flow gradients are expected to be the greatest, such as near the leading and trailing edges.

Governing Equations and Flow Solver

For flow about a body in the transonic regime with significant viscous effects and potential boundary-layer separations, the three-dimensional Navier–Stokes equations must be solved. In this study, the three-dimensional, thin-layer, Reynolds-averaged, Navier–Stokes equations are solved in generalized coordinates using the OVERFLOW code, reported by Buning et al.[11] This code is an outgrowth of the ARC3D[12] and F3D[13] codes previously developed at NASA Ames Research Center. The ARC3D algorithm option is used in this study. ARC3D is based on a three-factor scheme and uses central differencing in all three spacial directions with artificial smoothing (second- and fourth-order) to maintain stability. Because the flow is turbulent the Baldwin–Lomax turbulence model[14] with modifications from Degani and Schiff[15] that extend its applicability to flows with strong crossflow separation and strong vortices is used.

A grid sensitivity study is conducted to determine the grid density required to resolve the physical flow features of the transonic wing. Two grids are used in the study: a coarse grid consisting of 121 streamwise × 39 spanwise × 43 normal points and a refined density grid with 201 × 63 × 63 points. Solutions are obtained at freestream conditions of M_∞ = 0.82, $Re_{mac} = 6.0 \times 10^6$, and α = 1.5 deg to match the experimental conditions. The experimental and computed pressure distributions at three span locations are shown in Fig. 3. Both the coarse- and refined-grid results show the same trends as ob-

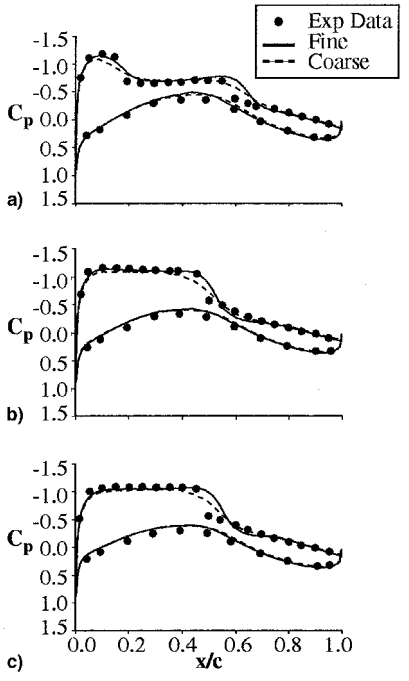

Fig. 3 Comparison of pressure distribution for coarse and refined grids; $M_\infty = 0.82$, $\alpha = 1.5$ deg, and $Re_{inc} = 6.0 \times 10^6$. η = a) 15, b) 50, and c) 70%.

served in the experimental data. Reference 9 shows that the effect of tunnel walls is to move the transonic shock forward in the experimental data. Also, the refined and coarse grids predict the transonic shock slightly aft of the experiment. Both grid cases and the experimental data show that at $\eta = 15\%$ span, there is a leading-edge suction peak that occurs roughly at $x/c = 0.1$. This is then followed by two shocks, one that occurs immediately after the suction peak and then one downstream at $x/c = 0.6$. There is good agreement on the lower surface of the wing as well. The other two span locations show similar trends with a shock located on the upper surface near $x/c = 0.5$ and good agreement of the lower surface. When comparing results using the two grid systems, the suction peak near the leading edge is better resolved by the refined grid. The shock is stronger and moves aft in the refined grid system; this creates additional lift. Furthermore, the refined-grid case shows a stronger transonic shock that is predicted to be slightly aft of the experimental data. This results in the lift coefficients being higher for the refined grid case. The C_L for the refined and coarse grids are $C_L = 0.516$ and 0.50, respectively, which is lower than the experimental value of $C_L = 0.53$. The experiment had a $L/D = 13.42$. To match C_L with either grid system the angle of attack in the computations would be increased. The angles of attack needed to match the experimental C_L value are $\alpha = 1.9$ and 1.6 deg for the coarse and refined grids, respectively.

There is a favorable comparison to the experimental data for both the refined and coarse grids. The coarse grid is used for optimization because of the computational time and memory constraints. Using the coarse grid decreases the amount of computational and wall clock time required, as well as allowing for more optimization runs given the available resources. Although not done in this study, a refined grid can be generated once an optimized geometry is found and an analysis can be performed to confirm the optimization.

Optimization Procedure

The optimization procedure begins with the optimizer generating a baseline objective function (the value or function that is being driven to the optimal minimum) from the initial values of the design variables. Then the optimizer perturbs each of the design variables to calculate the direction of the gradient using the previously obtained flow solutions. After each perturbation of the design variables, new surface and volume grids are created. OVERFLOW is called to solve the flow about the latest computational grid and then the objective function is calculated from this flow solution. Using OVERFLOW, the optimizer continues to perturb and search for the correct gradient direction until a set of design variables is found with a local minimum objective function. One of the major contributions of this study is the integration of a numerical optimization routine, NPSOL, with a grid generator and a validated flow solver, OVERFLOW. The total CPU time required for each iteration of the optimization routine on a Cray C-90 is 728.2 s of which 0.6, 99.25, and 0.05% is used by the grid generation process, flow solver, and the optimizer, respectively. The procedure just described is illustrated in Fig. 4.

Optimizer

The optimizer that is used in this study is NPSOL.[16] NPSOL is chosen as the optimizer because of past experience and its flexibility. Also, constraints can be easily implemented into the code. NPSOL is a collection of Fortran subroutines designed to solve the nonlinear programming problem stated as

$$\text{minimize} \quad F(\boldsymbol{x})$$

$$\text{subject to} \quad \boldsymbol{l} \leq \begin{bmatrix} \boldsymbol{x} \\ A\boldsymbol{x} \\ c(\boldsymbol{x}) \end{bmatrix} \leq \boldsymbol{u}$$

where $F(\boldsymbol{x})$ is the objective function, $\boldsymbol{x}$ is a vector of length n that contains the design variables, $c(\boldsymbol{x})$ contains the nonlinear constraint functions, and A is the linear constraint matrix. The variables $\boldsymbol{l}$ and $\boldsymbol{u}$ are the upper and lower bound vectors that must be specified for each design variable and constraint.

To locate the minimum of $F(\boldsymbol{x})$, the optimizer uses a sequential quadratic programming algorithm.[16] The search direction at each iteration is the solution of a quadratic programming problem. Each quadratic programming subproblem is solved by a quasi-Newton algorithm. The optimizer continues this process until it finds a local minimum of $F(\boldsymbol{x})$. The definition of $F(\boldsymbol{x})$, A, $c(\boldsymbol{x})$, and their bounds needs to be specified as inputs. The initial values of the design variables should also be supplied. An important consideration is the difference intervals. It should be noted that NPSOL has an option to calculate the difference interval used in the finite difference approximation of the gradient. However, this involves a large number of calls to the flow solver, which is too costly. For this reason, a common difference interval for all design variables is specified as an input throughout this study.

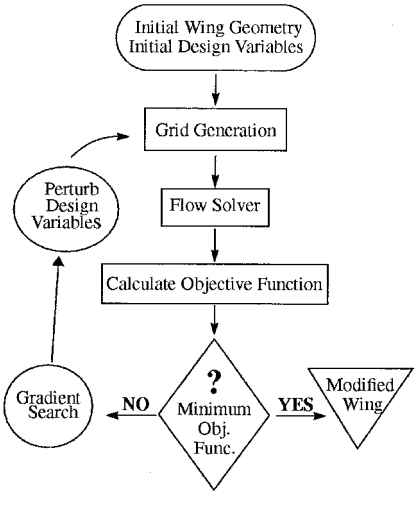

Fig. 4 Flow chart of the optimization procedure.

Design Variables and Nonlinear Constraints

Perturbations to the wing geeometry are performed through the use of design variables that have a direct influence on the objective function. The design variables that are chosen for this study help define the wing surface geometry. The three geometrical design variables that are used are the leading-edge sweep angle, the twist angle at the root chord, and the twist angle at the tip chord. These simple design variables are chosen so that the optimization procedure can be easily tested and the results can be readily explained. The sweep angle is expected to be the dominant design variable. In addition, the angle of attack is added as a fourth design variable in some optimization cases. A nonlinear constraint is placed on the flowfield by limiting the bounds of the lift coefficient.

Objective Function

At each step of the optimization process the optimizer alters the design variable values and a new wing shape is defined. A new computational grid is then generated and the flow solver calculates the flow over the new geometry. The objective function that is being minimized in this study is the D/L, which is the same as maximizing the L/D. The objective function is found by determining the C_D and the C_L by numerical integration of the pressure and skin friction over the entire body.

Results and Discussion

The NPSOL optimizer is used to find the optimized geometry that has the maximum L/D (minimizing D/L) for several cases with different design variables. The design variables that are studied include leading-edge sweep angle, twist angle at the root, and twist angle at the tip. OVERFLOW is used to solve the flowfield about the transonic wing at the baseline conditions for comparison with the optimal solutions. The original values of the wing design variables are $\Lambda = 27$ deg, $\theta_r = 2.76$ deg, and $\theta_t = -2.04$ deg. Optimization is performed with and without a constraint to limit the range of C_L, and the freestream flow conditions are $M_\infty = 0.82$, $\alpha = 1.9$ deg, and $Re_{mac} = 6.0 \times 10^6$ (based on freestream conditions and mean aerodynamic chord). The angle of attack is chosen so that the baseline solution has the experimental value of $C_L = 0.53$. In all cases presented, the computed flow is treated as fully turbulent except near the leading edge (approximately $x/c = 0.03$ as defined in the experiment) to approximate transition.

Single-Design Variable Study

To better understand the effects of each geometric parameter individually, an initial study is conducted to optimize only one design variable at a time while the other design variables are held fixed at their baseline values. The optimal value of the design variable is found by maximizing L/D without a lift constraint and by setting upper and lower bounds on the design variables. Table 1 shows the values of the original and modified design variables for the single-parameter case study. The optimization process is converged at 8, 15, and 13 iterations for the sweep, twist angles at the root and tip, respectively. Because increasing sweep at constant t/c and C_L decreases drag, the optimizer fixes sweep at the upper bound as expected. Although improved L/D could be obtained with higher sweep angles, structural and stability considerations would limit such high-sweep angles. The higher swept wing has a reduced effective Mach number that essentially reduces the local Mach number inside the supersonic region. Thus, the shock-wave strength is lowered and the effects on boundary-layer separation will be less severe. This is one of the explanations of why the sweep angle tends to increase toward the upper bound.

Table 1 Single-design variable study

Case	Original, deg	Lower bound, deg	Upper bound, deg	Modified, deg
Sweep	27	10	40	40
Root twist angle	2.74	−5	10	0.667
Tip twist angle	−2.04	−10	5	−6.199

Both twist angles at the root and tip are optimal at values between the lower and upper bounds. In each case the optimized lift coefficient is lower than the original value, as shown in Table 2. A wing, however, is often required to have a certain C_L for proper lift at takeoff or cruise conditions. Thus, a second study is conducted using OVERFLOW to investigate what angle-of-attack adjustments would be needed to recover the original lift coefficient in each case. In the current case the new angle of attack is always higher than the original because the lift needs to be increased. As seen in Table 2, the L/D decreases when the angle of attack is increased to recover the original C_L. When the angle of attack is increased, both the drag and the lift increase and the overall effect is to lower the L/D. The sweep case is the only modified case for individual parameters that has a higher L/D than the original wing when the angle of attack is increased to match C_L.

To get a better understanding of the flow physics, the pressure distribution and the upper surface pressure contours are examined and compared to the original wing A. To compare pressure distributions, the pressure distribution for the original wing is recomputed at $\alpha = 1.9$ deg and the modified wing at the corresponding angle of attack to match the experimental C_L, as shown in Table 2. Therefore, the lift coefficient for both geometries is equal, $C_L = 0.53$. The pressure distribution for each case is compared to the original wing at three span locations, $\eta = 15$, 50, and 70% as shown in Fig. 5. First, the sweep case shows that the modified wing suction peak is larger than the original, which allows more lift to be created near the leading edge. The shock position has clearly moved forward in the sweep case from roughly $x/c = 0.6$ to 0.25 as is shown at $\eta = 50$ and 70%. This effect results in increased leading-edge suction that serves to decrease drag at this lift coefficient. In the next case, the twist angle at the root is changed from the original case. Figure 5b shows that there is a slight decrease in the suction peak at $\eta = 15\%$. In the last case, with the design variable chosen to be twist angle at the tip, the suction peak at $\eta = 15\%$ is slightly higher and the shock position is moved aft slightly. There is no noticeable change at $\eta = 50\%$ and at the last span location, the suction pressure is decreased near the leading edge. Basically, after correcting the angle of attack, the modified twist at the root (decreasing θ_r) produces a wash-in effect, whereas the twist at the tip (decreasing θ_t) generates a washout effect. This result indicates that twist at the root and tip cannot be further independently optimized to improve L/D at constant lift.

Table 2 Alpha correction for single-design variable study

Case	α, deg	C_L	L/D ($L/D_{orig} = 15.54$)	% Improvement of L/D
Sweep	1.9	0.404	21.17	36.9
	3.4	0.53	15.88	2.2
Root twist angle	1.9	0.325	19.97	28.5
	3.5	0.533	15.50	−0.3
Tip twist angle	1.9	0.40	17.95	15.5
	2.94	0.535	14.97	−3.7

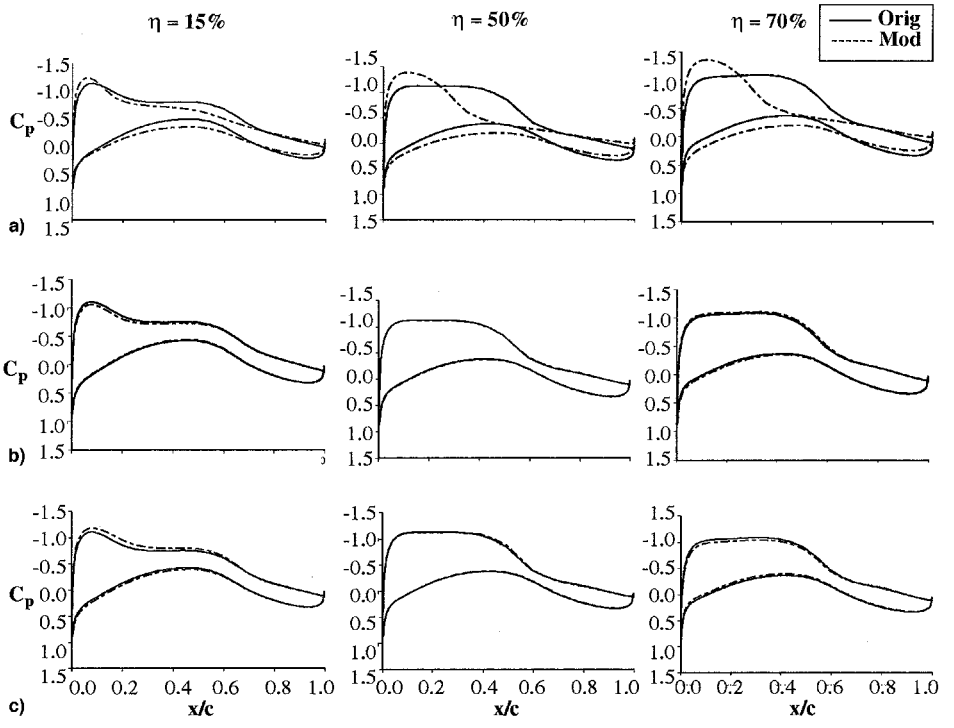

Fig. 5 Pressure distribution for single-design variable study: a) sweep, b) root twist angle, and c) tip twist angle.

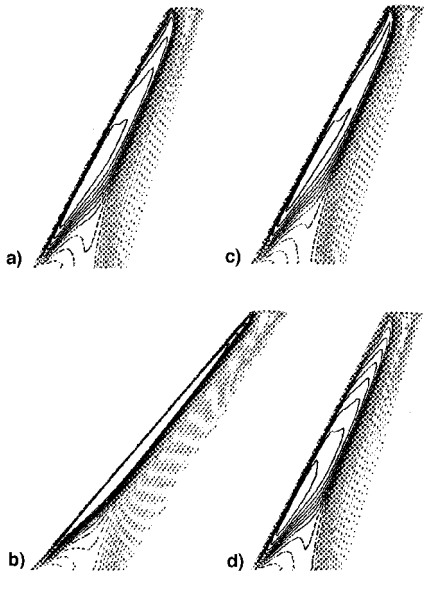

Fig. 6 Surface pressure contours for single-design variable study: a) original, b) sweep angle, c) twist angle at the root, and d) twist angle at the tip.

The surface pressure contours for the single-design variable cases are compared to the original wing and are shown in Fig. 6. This figure correlates with the preceding description of the changes observed in the flowfields of the optimized cases. The double shock that was seen in Fig. 5 is also seen in the surface pressure contours of the inboard wing. In addition, the movement of the shock positions in the modified cases are also clearly seen. In the original wing the suction pressure is shown in black at the leading edge and extends just past the midspan of the wing. Near the trailing edge there is a higher pressure region shown in gray. The modified sweep case shows that the shock position has moved forward to approximately a quarter-span. For the twist angles at the root and tip cases there appears to be no significant changes in the shock positions as seen in Figs. 5b and 5c. There is also no noticeable change in the pressure contours aft of midspan and at the trailing edge. There are small changes in the pressure at the root and tip; this is also seen in Fig. 5.

Multiple-Design Variables

Although insight can be gained by studying individual parameters, the effects of geometric parameters on the aerodynamics are generally nonlinear. To better understand the flow about the transonic wing and how each geometric parameter is affected by one another, an optimization study is conducted using multiple-design variables. The first case is to activate all three design variables at the same time and use the optimal values from the single-design variable cases as the starting values. Again, there is no constraint on lift. The lower and upper bounds are the same for each design variable as in the single-design variable study as shown in Table 2. This case is converged with 29 iterations. The optimal values are found to be $\Lambda = 40.00$ deg, $\theta_r = 1.397$ deg, and $\theta_t = -2.54$ deg, as shown in Table 3. This case will be referred to as case A. The sweep angle is increased from the original value and is optimal at the upper bound. As expected, the sweep was the dominant design variable in this study. Both twist angles decreased from the original values. The lift-to-drag ratio is increased to $L/D = 23.41$, which is a 51% increase from the original wing. The lift and drag coefficients of the modified wing are $C_L = 0.30$ and $C_D = 0.013$, as shown in Table 3. To recover the lift the freestream angle of attack is increased until the C_L matches the original value of $C_L = 0.53$. This value is found to be $\alpha = 4.53$ deg and this case will be referred to as case B. At these new freestream conditions, the L/D changes to $L/D = 16.26$ and C_D increases to $C_D = 0.033$. L/D still retains a significant increase of 4.6% from the original value and is higher than any of the single-design variable optimizations (Table 2). Although sweep is the dominant design variable it is clear that the best results are obtained when the root and tip twist angles are included in the optimization.

The pressure distribution is shown in Fig. 7 and will be used to understand why the design variables are moved in the particular directions by the optimizer. To compare pressure distributions the pressure distribution for the original wing is computed at $\alpha = 1.9$ deg and the modified wing at $\alpha = 4.53$

Table 3 Multiple-design variable study

Case	Design variables $\begin{bmatrix}\Lambda\\ \theta_r\\ \theta_t\end{bmatrix}$	α, deg	C_L	C_D	L/D	% L/D improvement over baseline
Original	$\begin{bmatrix}27\text{ deg}\\ 2.74\text{ deg}\\ -2.04\text{ deg}\end{bmatrix}$	1.9	0.53	0.034	15.54	——
Three-design variable No constraint Case A	$\begin{bmatrix}40.0\text{ deg}\\ 1.397\text{ deg}\\ -2.54\text{ deg}\end{bmatrix}$	1.9	0.30	0.013	23.36	50.3
Optimal three-design variable α-cor. Case B	$\begin{bmatrix}40.0\text{ deg}\\ 1.397\text{ deg}\\ -2.54\text{ deg}\end{bmatrix}$	4.53	0.53	0.033	16.26	4.63
Four-design variable Constraint lift Case C	$\begin{bmatrix}40.00\text{ deg}\\ 1.386\text{ deg}\\ -2.54\text{ deg}\end{bmatrix}$ $\alpha = 4.517$ deg	4.517	0.53	0.032	16.31	4.96

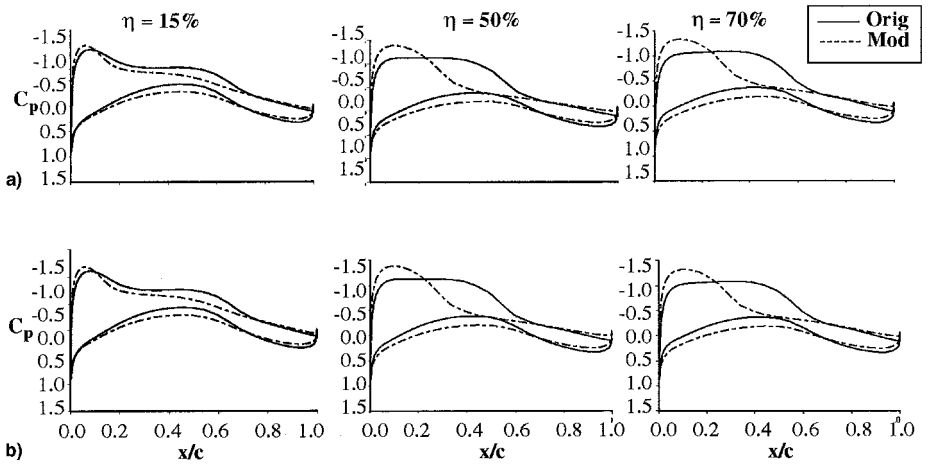

Fig. 7 Pressure distribution for multiple-design variables study: a) three-design variables, case B; and b) four-design variables, case C.

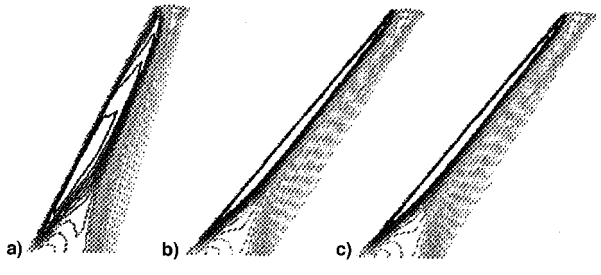

Fig. 8 Surface pressure contours for multiple-design variable study: a) original; b) three-design variables, case B; and c) four-design variables, case C.

deg. The lift coefficient for both geometries are equal, C_L = 0.53. At the first span location, η = 15%, the modified wing has a very small increase in the suction peak. The shock position moves slightly forward. Greater changes are observed at the other span locations. At η = 50% the suction peak is larger and the shock has moved forward by about 20% chord. The C_p plot at the next span location shows that the suction peak is greater than the original wing. Because the leading-edge suction is greater in the modified wing, the lift generated is higher and the drag is reduced. Additional lift comes from a higher pressure on the lower surface.

The corresponding surface pressure contours are shown in Fig. 8. When case B is compared to the original wing it is seen that the shock position moves forward at midspan from approximately midchord to quarterchord. The shock position also moves forward about the same distance near the tip of the wing. Drag reduction is obtained as a result of stronger leading-edge suction pressures for the modified wing. Near the wing root the double-shock pattern shown by the contours indicate a weakened aft shock for the modified case. This effect is also observed in the C_p plots of Fig. 7. Contours show little difference between the two modified cases.

To refine the attempted optimization process several different methods were tried to increase the L/D using multiple-design variables. It was found that the best method adds the angle of attack as a design variable and constrains the lift. The initial values of the design variables are the optimal values from case B with the initial value for the angle of attack of α = 4.53 deg. The lower and upper bounds are the same as in the previous case for the geometric parameters and the angle of attack is bounded by 0 deg < α < 8 deg. This case will be referred to as case C and is converged with 17 iterations. The optimized values for case C are quite close to the values obtained for case B. The angle of attack is optimal at α = 45.17 deg. L/D is increased to L/D = 16.31, which is almost a half of a percent increase from case B. However, when compared to the original case, there is an increase of 5%. The pressure distribution, shown in Fig. 7b, is almost identical to case B as is the surface pressure distribution shown in Fig. 8c. It should be noted that the optimizer did not perturb the geometry when the lift is constrained and the original values of the design variables are picked as the starting values. In other words, the optimizer could not find a feasible search direction within the bound of the lift constraints. Thus, to get the optimizer moving on a constrained run and to fine-tune the optimization, the

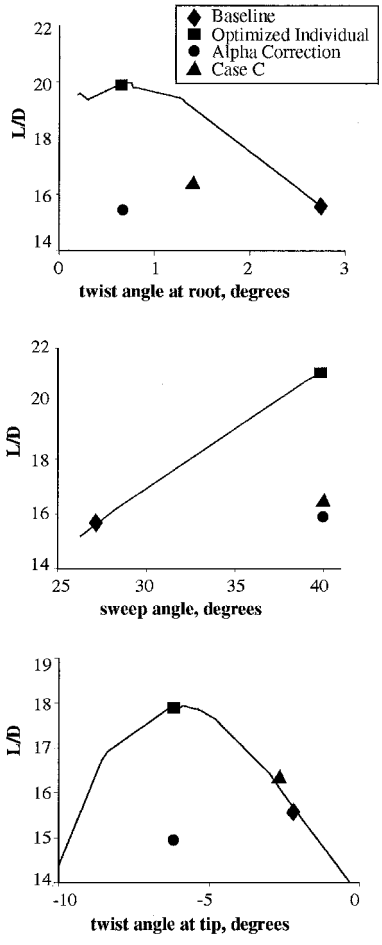

Fig. 9 Sensitivity plots of design variables in *L/D*.

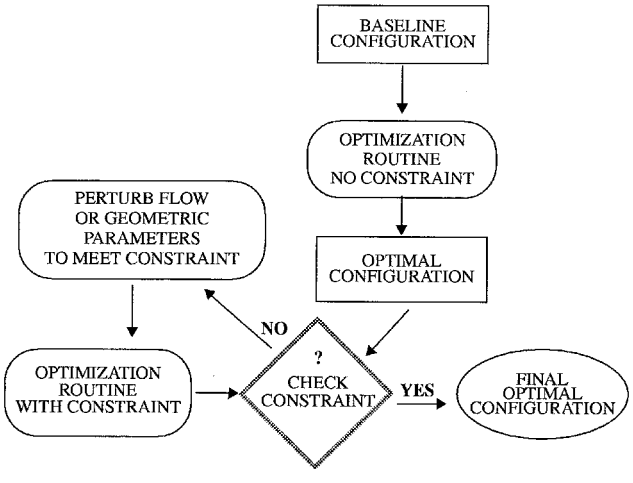

Fig. 10 Overall optimization routine flow chart.

results from case B are used as the starting values for the design variables and the lift is constrained.

Optimization Method

The design space of the individual design variables is studied to better understand how they affect the *L/D*. The individual design spaces for sweep angle, twist angles at the root and tip are complex and are shown in Fig. 9. The solid curve is the design map for the individual design variables. The diamonds represent the baseline values for each design variable. The squares represent the optimal value that is found for the original α = 1.9 deg. The circles represent the optimal value at the *L/D* for the corresponding angle of attack that is needed to recover the experimental C_L (refer to Table 2). The sweep angle has a nearly linear design space in *L/D*. The maximum *L/D* occurs at the upper bound for sweep angle. Both twist angles at the root and tip have nonlinear paths in the design space. The optimal values for the specified bounds are shown in Fig. 9 with the corresponding squares. For reference, the triangles represent the optimal value that is found from the procedure that uses four design variable with a constraint on lift (case C).

There is no clear path for obtaining the overall optimal values of each design variable by optimizing each one independently because of the nonlinear effects of the design variables on the aerodynamics. When the angle of attack is corrected to match the required value of C_L, the *L/D* for the single-variable cases is significantly lower than when optimizing the design variables together with the addition of angle of attack as a variable. It should also be noted that the angle of attack does not need to be fed into the optimization loop but can be corrected afterward using the flow solver.

There are many paths that can be chosen to find the optimal objective function. For instance, some choices that need to be made include the number of design variables, the types of constraints, and the use of flow conditions as design variables. In this study, the optimal objective function value is reached using multiple-design variables, constraining aerodynamic parameters, and including a flow condition (angle of attack) as a design variable. Figure 10 summarizes the procedures that are used for this optimization. The basic optimization routine, which includes the grid generation, flow solver, and the gradient search, is illustrated in Fig. 4. Once an initial estimate of the optimal configuration is found a constraint or additional constraints are placed on the solution to focus in on the final optimal configuration. Another option would be to add design variables, either geometric or flow conditions, to force the optimizer to find yet a better configuration. Once all constraints and design parameters are met, the final configuration is optimized.

Conclusions

A tool is developed to aid in optimizing and understanding the characteristics of a transonic wing. A designer can develop a better understanding of the related flow physics and design a better performing wing. A numerical optimization routine is integrated with a grid generator and a validated Navier–Stokes flow solver. The effects of wing sweep angle, root and tip twist angles, and angle of attack on the *L/D* are studied using surface pressure contours and pressure distributions. The results of this paper show that when the *L/D* is increased using single-design variable optimization, the resulting lift coefficient falls below the original value. The angle of attack must be increased to preserve the original lift coefficient with the modified geometry. The optimal configuration with the highest *L/D* is found by first optimizing with multiple-design variables, then including the angle of attack in the design loop with lift constrained to the original value. Thus, proper optimization may require a series of local optimization and angle-of-attack adjustments. It was also found that multiple-design variable optimization yielded improved results over a single dominant design variable.

References

[1]Dulikravich, G., "Aerodynamic Shape Design and Optimization: Status and Trends," *Journal of Aircraft*, Vol. 29, No. 6, 1992, pp. 1020–1026.

[2]Van den Dam, R. F., Van Egmond, J. A., and Slooff, J. W., "Optimization of Target Pressure Distributions," Special Course on Inverse Methods for Airfoil Design for Aeronautical and Turbomachinery Applications, AGARD Rept. 780, Ref. 3, Nov. 1990.

[3]Obayashi, S., and Takanashi, S., "Genetic Optimization of Target Pressure Distributions for Inverse Design Methods," AIAA Paper 95-1649, June 1995.

[4]Cheung, S., Aaronson, P., and Edwards, T., "CFD Optimization of a Theoretical Minimum-Drag Body," *Journal of Aircraft*, Vol. 32, No. 1, 1995, pp. 193–198.

[5]Cosentino, G. B., and Holst, T. L., "Numerical Optimization of Advanced Transonic Wing Configurations," *Journal of Aircraft*, Vol. 23, No. 3, 1986, pp. 192–199.

[6]Ta'asan, S., Kuruvila, G., and Salas, M. D., "Aerodynamic Design and Optimization in One Shot," AIAA Paper 92-0025, Jan. 1992.

[7]Reuther, J., and Jameson, A., "Control Theory Based Airfoil Design for Potential Flow and a Finite Volume Discretization," AIAA Paper 94-0499, Jan. 1994.

[8]Reuther, J., and Jameson, A., "Aerodynamic Shape Optimization of Wing and Wing-Body Configurations Using Control Theory," AIAA Paper 95-0123, Jan. 1995.

[9]Hinson, B. L., and Burdges, K. P., "Acquisition and Application of Transonic Wing and Far-Field Test Data for Three-Dimensional Computational Method Evaluation," U.S. Air Force Office of Scientific Research, TR-80-0421, March 1980.

[10]Chan, W., and Steger, J., "A Generalized Scheme for Three-Dimensional Hyperbolic Grid Generation," AIAA Paper 91-1588, June 1991.

[11]Buning, P. G., Chan, W. M., Renze, K. J., Sondak, D. L., Chiu, I., Slotnick, J. P., Gomez, R. J., Jespersen, D. C., Krist, S. E., and Rizk, Y. M., "OVERFLOW Manual Version 1.6bc," NASA Ames Research Center, Moffett Field, CA, Nov. 1995.

[12]Pulliam, T. H., and Steger, J. L., "Implicit Finite Difference Simulations of Three-Dimensional Compressible Flow," *AIAA Journal*, Vol. 18, No. 2, 1980, pp. 159–167.

[13]Steger, J. L., Ying, S. X., and Schiff, L. B., "A Partially Flux-Split Algorithm for Numerical Simulation of Compressible Inviscid and Viscous Flow," *Proceedings of the Workshop on Computational Fluid Dynamics*, Inst. of Nonlinear Sciences, Univ. of California, Davis, CA, July 1986.

[14]Baldwin, B., and Lomax, H., "Thin-Layer Approximation and Algebraic Model for Separated Turbulent Flows," AIAA Paper 78-257, Jan. 1978.

[15]Degani, D., and Schiff, L. B., "Computation of Turbulent Supersonic Flows Around Pointed Bodies Having Crossflow Separation," *Journal of Computational Physics*, Vol. 86, No. 1, 1986, pp. 173–196.

[16]Gill, P., Murray, W., Saunders, M., and Wright, M., "User's Guide for NPSOL: A Fortran Package for Nonlinear Programming," Dept. of Operations Research, Stanford Univ., TR SOL 86-2, Stanford, CA, 1986.